Check for updates

ARTICLE   OPEN

Synechococcus nitrogen gene loss in iron-limited ocean regions

Garrett Sharpe[1], Liang Zhao[2], Meredith G. Meyer[2], Weida Gong [2], Shannon M. Burns [3], Allesandro Tagliabue [4], Kristen N. Buck[3,5], Alyson E. Santoro[6], Jason R. Graff[7], Adrian Marchetti [2] and Scott Gifford [2✉]

Synechococcus are the most abundant cyanobacteria in high latitude regions and are responsible for an estimated 17% of annual marine net primary productivity. Despite their biogeochemical importance, *Synechococcus* populations have been unevenly sampled across the ocean, with most studies focused on low-latitude strains. In particular, the near absence of *Synechococcus* genomes from high-latitude, High Nutrient Low Chlorophyll (HNLC) regions leaves a gap in our knowledge of picocyanobacterial adaptations to iron limitation and their influence on carbon, nitrogen, and iron cycles. We examined *Synechococcus* populations from the subarctic North Pacific, a well-characterized HNLC region, with quantitative metagenomics. Assembly with short and long reads produced two near complete *Synechococcus* metagenome-assembled genomes (MAGs). Quantitative metagenome-derived abundances of these populations matched well with flow cytometry counts, and the *Synechococcus* MAGs were estimated to comprise >99% of the *Synechococcus* at Station P. Whereas the Station P *Synechococcus* MAGs contained multiple genes for adaptation to iron limitation, both genomes lacked genes for uptake and assimilation of nitrate and nitrite, suggesting a dependence on ammonium, urea, and other forms of recycled nitrogen leading to reduced iron requirements. A global analysis of *Synechococcus* nitrate reductase abundance in the TARA Oceans dataset found nitrate assimilation genes are also lower in other HNLC regions. We propose that nitrate and nitrite assimilation gene loss in *Synechococcus* may represent an adaptation to severe iron limitation in high-latitude regions where ammonium availability is higher. Our findings have implications for models that quantify the contribution of cyanobacteria to primary production and subsequent carbon export.

ISME Communications; https://doi.org/10.1038/s43705-023-00314-9

INTRODUCTION

Prochlorococcus and *Synechococcus* are critical components of marine biogeochemical cycles, generating ~25% of the ocean's annual net primary production and contributing significantly to carbon export [1, 2]. *Prochlorococcus* is largely restricted to equatorial and subtropical latitudes, while *Synechococcus* dominates cooler waters in regions of equatorial upwelling and high latitudes [3]. Both groups exhibit high levels of strain diversification due to niche specialization arising from variations in environmental conditions (light, temperature, nitrogen, phosphorus, etc.) including iron availability [4–6].

Iron (Fe) is an essential micronutrient as it is a required cofactor in photosynthetic and respiratory electron transport chains [7, 8]. Photosystems I and II require 12 and 3 iron atoms per photosystem, respectively, and the light-harvesting phycobilisome proteins are synthesized by iron-containing enzymes [8]. Iron is also required in other key metabolic functions, including nitrate and nitrite assimilation, with nitrate and nitrite reductases requiring 4 and 5 iron atoms per enzyme, respectively [9–11]. In High Nutrient Low Chlorophyll (HNLC) regions these cellular iron demands in combination with low iron bioavailability lead to iron limitation of primary production. Three major ocean regions have been identified as HNLC zones: the Equatorial Pacific, the Southern

Ocean, and the subarctic North Pacific; together they represent roughly 30% of the world's oceans [12]. These regions are characterized by low phytoplankton biomass and consistently high concentrations of macronutrients in the mixed layer resulting from incomplete utilization due to severe iron limitation [13, 14]. Nitrate (NO_3^-) concentrations for example are in the tens of micromolar range [14].

Synechococcus and *Prochlorococcus* strains have evolved diverse adaptations to iron limitation. In non-HNLC regions, *Prochlorococcus* are enriched in iron-storing ferritin genes and iron uptake regulators that enables growth at approximately tenfold lower iron concentrations and a more rapid response to iron-stress relief, and low-light adapted *Prochlorococcus* also often possess siderophore transport operons in order to scavenge for iron at the deep chlorophyll maximum where competition for iron is more intense [15, 16]. In *Synechococcus*, a study comparing the Atlantic coastal strain WH8020 to the oligotrophic ocean strain WH8102 found that coastal strain WH8020 possesses multiple iron storage, stress regulation, and response genes that are intricately regulated under the dynamic iron conditions of the coastal environment [17]. By contrast, the pelagic *Synechococcus* strain WH8102 that was isolated from the primarily nitrogen-limited Sargasso Sea oligotrophic gyre lacks many of these

iron-response genes and exhibit a more limited iron regulatory response [17].

Cyanobacteria, however, are relatively under-sampled in high-latitude HNLC regions, resulting in a major gap in understanding nutrient acquisition and adaptation strategies in these large, biogeochemically important regions. In tropical and subtropical HNLC regions, *Prochlorococcus* and *Synechococcus* have adapted to iron-limiting conditions by substituting iron requiring genes such as iron-sulfur (Fe-S) containing proteins with non-iron containing functional homologues [18, 19]. Several *Synechococcus* strains from the CRD1 and CRD2 clades, two phylogenetically distinct lineages of *Synechococcus* found in the equatorial Pacific HNLC region, exhibit adaptations to iron limitation such as high ferritin gene copy numbers (CRD1), multiple types of iron transporters (CRD1), and siderophore uptake (CRD2) [19, 20]. Although no members of these clades have yet been isolated or sequenced from outside of the equatorial Pacific, 16S-23S internally transcribed spacer (ITS) marker gene analysis has shown that members of the CRD1 and CRD2 clades, are also present in high-latitude HNLC waters [20]. These HNLC regions are not well represented in current bacterial metagenomic datasets, and all currently sequenced isolates, metagenome-assembled genomes (MAGs), and single cell assembled genomes (SAGs) from these clades are derived from low-latitude HNLC zones [2, 20–23].

The absence of high-latitude HNLC *Synechococcus* genomes leaves a substantial gap in our current knowledge of picocyanobacterial iron adaptation strategies and their importance to biogeochemical cycling. Here, we used quantitative metagenomics and genome assembly to enumerate and characterize cyanobacteria populations at Station P (Ocean Station Papa) to identify the strategies *Synechococcus* have evolved to succeed in iron-limited HNLC zones and their impact on biogeochemical cycling and carbon export.

METHODS

Samples were collected at Station P in the North Pacific in August and September 2018 as part of the NASA Export Processes in the Ocean from RemoTe Sensing (EXPORTS) expedition [24]. Flow cytometric enumeration of *Synechococcus* was performed on a Becton Dickinson Influx Cell Sorter (BD-ICS) flow cytometer while at sea following previously published protocols [25]. For uptake incubations, seawater was collected with a trace metal clean rosette, aliquoted into acid washed bottles, and inoculated with $NaH^{13}CO_3$ isotope and $Na^{15}NO_3$ isotope at 10% of ambient dissolved inorganic carbon (DIC) and NO_3^- concentrations and incubated for 24 hours. Samples were gravity filtered through pre-combusted GF/F filters, dried and stored until onshore analysis at the University of California Davis Stable Isotope Facility [26]. Ambient nutrient concentrations were collected as described in Siegel et al. 2021 [24].

For the metagenomes, seawater was prefiltered through a 5 μm polycarbonate membrane filter and cells collected on 0.2 μm polyethersulfone (PES) membrane filter. DNA for short read sequencing was extracted from the filters using a DNeasy Powerwater kit. Three internal genomic standards were added immediately before starting the extraction. Metagenomes were sequenced with HiSeq 4000 as 2 ×150 bp reads, and can be accessed under the NCBI Bioproject PRJNA78533 (Biosamples 24695624-24695646). Metagenome reads were annotated with a DIAMOND search against the NCBI Refseq protein database [27]. Metagenome assembled genomes (MAGs) were assembled with metaspades and then mapped for read coverage with Bowtie2 [28, 29]. Contigs were each binned by MetaBAT, MaxBin, and CONCOCT, and then consolidated using DAS Tool and CheckM [30–35]. *Synechococcus* MAG quality was increased by performing several additional assemblies including Oxford nanopore long reads and manual curation (See supplemental for detailed methods). DNA for long read sequencing was obtained by phenol chloroform extraction. These Whole Genome Shotgun projects have been deposited at DDBJ/ENA/GenBank under the accessions JAVBIW000000000 for *Synechococcus* sp. SP1 and JAVBIX000000000 for *Synechococcus* sp. SP2.

Synechococcus volumetric abundances were derived from internal standard normalized metagenomes by *recA* and internal standard genome recovery as described in Gifford et al. [36] and Satinsky et al. [37].

Metagenome *recA* genes were identified by a DIAMOND homology search against a custom RecA protein database, and the resulting *recA* read counts were converted to volumetric abundances using the internal standard's recovery ratio and volume of seawater filtered.

To calculate MAG volumetric abundances, a coverage-based ratio was calculated for each of the three internal standard genomes by mapping metagenome reads to the internal standard reference genomes. The coverage-based recovery ratio is derived via the following:

$$R_{cov} = \frac{S_{cov}}{S_a} \qquad (1)$$

$$M_a = \frac{M_{cov}}{R_{cov}} \qquad (2)$$

(1) R_{cov}: coverage-based recovery ratio.
   S_{cov}: mean depth of coverage of internal standard genomes by metagenomic reads.
   S_a: molecules of internal standard genomes added to the sample
(2) M_a: molecules of any genome (MAG) in the sample.

M_{cov}: mean depth of coverage of any genome (MAG) in the sequence library.

Metagenomic reads were mapped onto the internal standard genomes with bowtie2 and the mean depth of coverage was calculated by dividing the total number of bases mapped by the size of the genomes. The mean depth of coverage represents the number of internal standard genome recovered through sequencing, and this was divided by the number of genomes added to the samples to get at the recovery ratio. The number of MAGs recovered from the sequence library was retrieved by mapping reads onto the MAG and calculating mean depth of coverage. The *Synechococcus* MAG volumetric abundances were then determined by mapping metagenome reads onto the *Synechococcus* MAG, calculating the mean depth of coverage, and then dividing by the coverage-based recovery ratio and volume of seawater filtered.

For comparison of *Synechococcus* nitrogen gene frequencies between our metagenomes and TARA metagenomes, nitrogen gene (nitrate reductase, nitrite reductase, and ammonia transporter) to *recA* ratios were calculated using the TARA 0.2–3.0 μm fraction at 5 m for each TARA Station. The raw TARA metagenome reads were processed in the same manner as the Station P metagenome dataset. A diamond search against NarB, FocA, Amt, and RecA-specific NCBI refseq databases narrowed down the gene hits, and a following diamond BLAST of the resulting gene hits against the entire NCBI refseq v95 databased eliminated false positive hits. For *recA*, an additional diamond search against the GTDB RecA database was used to obtain GTDB taxonomic identifications. *Synechococcus* nitrogen and recombinase A genes were pulled out of the total hits, and hits with *Synechococcus* annotations in both NCBI and GTDB were quantified and used to calculate the nitrogen gene to *recA* ratios. Detailed descriptions of sample collection, processing, and all bioinformatic analysis can be found in the supplemental methods.

RESULTS AND DISCUSSION

Station P is a low productivity system with high nitrate (7–15 μM) and low iron (<100 pM) concentrations characteristic of HNLC regions [13, 38, 39]. Phytoplankton blooms are rare, and primary production is sustained primarily by intrusion of nutrients from the shallow seasonal pycnocline [40]. Fitting with previous observations, phytoplankton at Station P during our sampling consisted primarily of small cells (<5 μm), including *Synechococcus*, small pennate diatoms, and autotrophic flagellates, with low abundance of large (>5 μm) flagellates and diatoms (Fig. 1). Correspondingly, the small size fraction had the highest chlorophyll concentrations, carbon, nitrate, and ammonium uptake rates, and represented 68% of total primary production (Fig. 1). The f-ratios (fraction of total primary production fueled by nitrate: here nitrate uptake/[nitrate + ammonium uptake]) were low for both size fractions, though the small cells had f-ratios half that of the large cells (Fig. 1). Together, the relatively low primary production and f-ratios observed at Station P indicate a system driven by
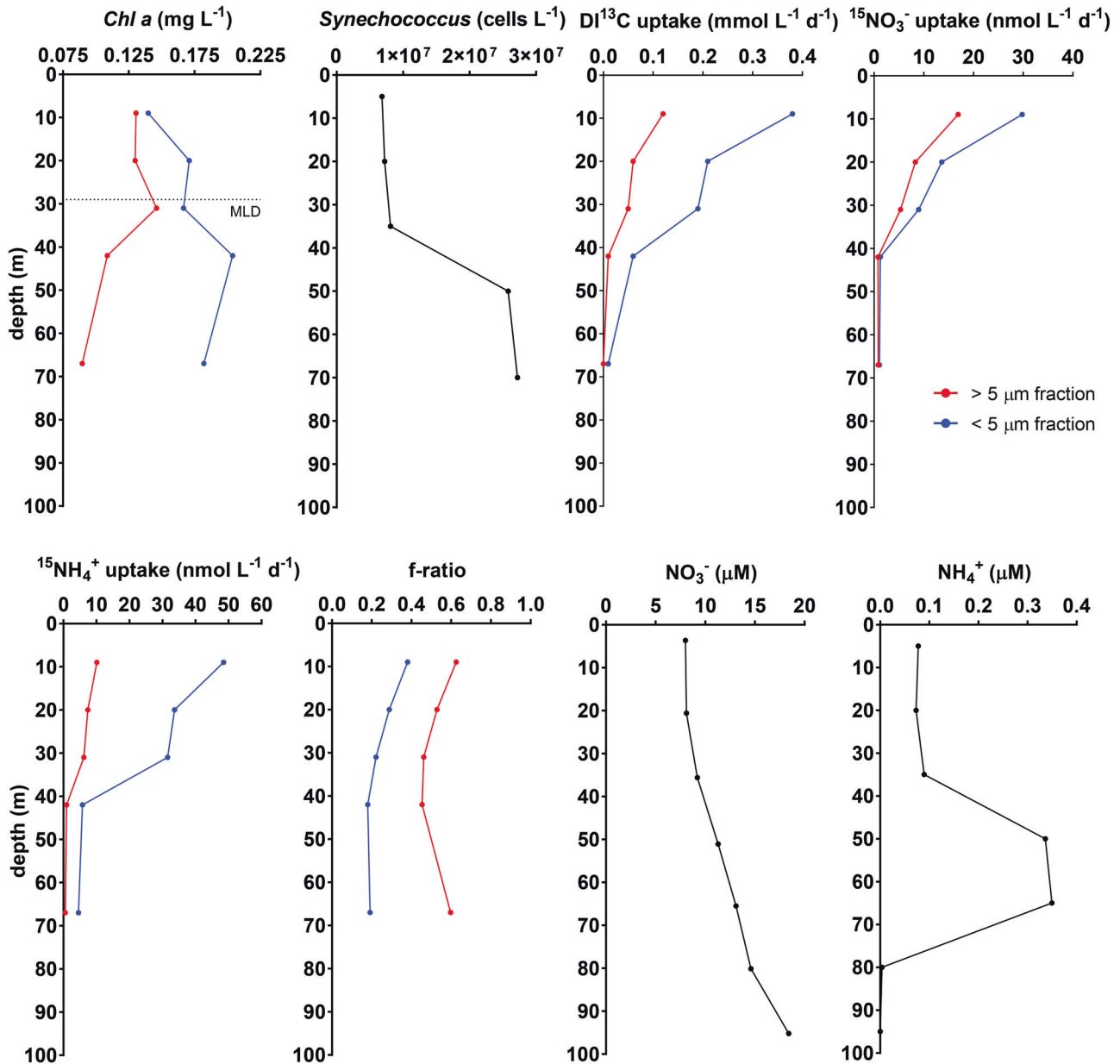
Fig. 1 Depth distributions of biological, nutrient, and uptake rates at Station P, September 7th 2018. Chl a Chlorophyll a, ^{13}C uptake radiolabeled carbon uptake rates, $^{15}NO_3^-$ uptake nitrate uptake rates, NH_4^+ uptake ammonium uptake rates. f-ratios calculated from the upper 100 m of the water column for the >5 μm (red) and <5 μm (blue) phytoplankton fraction. Nitrate (NO_3^-) and ammonium (NH_4^+) concentrations. Average mixed layer depth (MLD) for the cruise (29 m +/− 4.5 m) is indicated in *Chl-a* graph.

regenerated production, particularly by small phytoplankton cells [24, 26, 41].

The *Synechococcus*-dominated deep chlorophyll maximum (DCM) was located at 50–70 m, below the mixed layer but above the ferricline, which was around 200 m (Supplementary Fig. S1). Additionally, iron inputs from dust deposition and mesoscale eddy events are infrequent at Station P compared to the adjacent subtropical North Pacific Gyre, and surface dissolved iron concentrations were low (<0.03 nM in 14 of 24 surface samples collected during the cruise; seasonally: ~0.05 nM spring and summer, ~0.1 nM winter) [41–45]. Ammonium and nitrate concentrations were relatively high at all sampled depths, suggesting neither oxidized nor reduced forms of nitrogen are limiting (Fig. 1 and Supplementary Fig. S2).

We used quantitative metagenomics to enumerate *Synechococcus* abundances at Station P. Genome equivalents were

enumerated by identifying single copy recombinase A (*recA*) genes in a metagenome sample, and then converted to volumetric abundances via recovery ratios derived from internal standards added prior to extraction [36, 45–50]. A comparison between our quantitative metagenome-derived *Synechococcus* abundances and simultaneously collected flow cytometry *Synechococcus* cell concentrations show strong agreement (Fig. 2A), further supporting the use of internal standard quantitative metagenomics for determining absolute abundances of bacterial groups *in situ*. *Synechococcus* were the most abundant cyanobacteria at all depths (Fig. 2B), with peak densities of 5×10^7 cells L^{-1} at 50–75 m (Fig. 2B). Taxonomic classification of the *recA* genes revealed the *Synechococcus* community was dominated by two populations, Clade I and IV, both previously found to be abundant at other high-latitude sites [18, 22, 51, 52]. These two clades represented >99% of the Station P *Synechococcus*
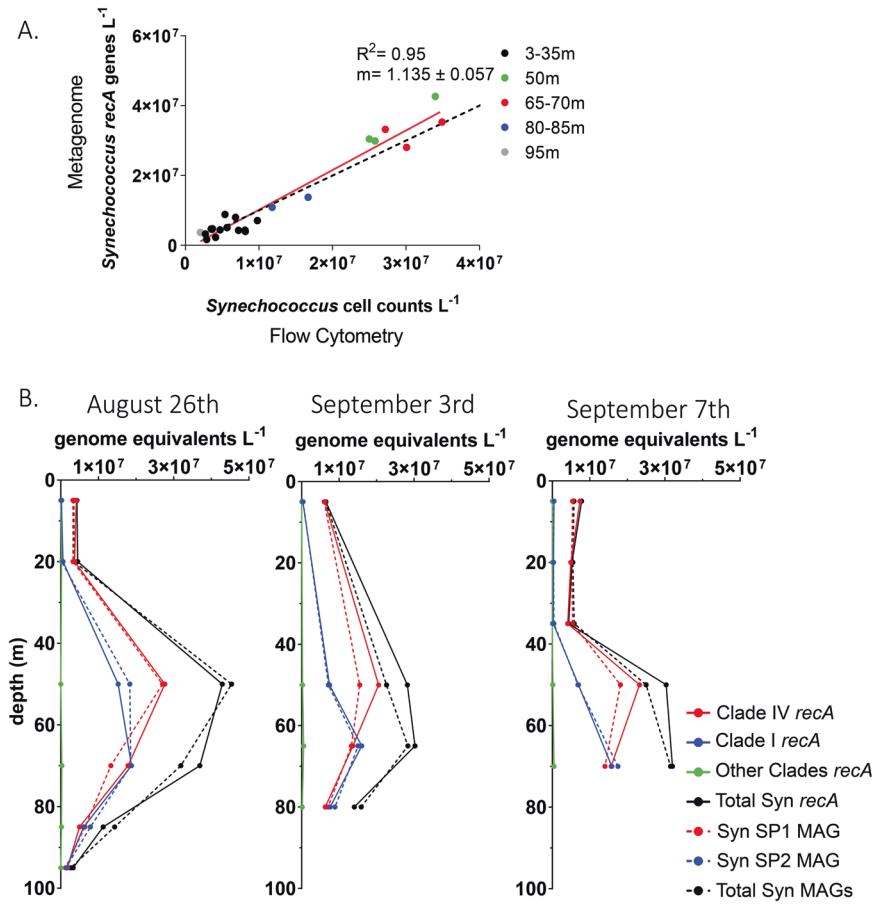
Fig. 2 Metagenome-derived volumetric abundances of total *Synechococcus* cells and *Synechococcus* MAG populations at Station P.
A Comparison of flow cytometry versus metagenome derived *Synechococcus* abundances. The red line is the linear regression model, and the black dashed line is the 1:1 line. **B** Metagenome-derived depth distributions of total *Synechococcus* cells, the subset of *Synechococcus* Clade I and IV populations, and the abundances of cells represented by the three different MAGs. *recA* abundances (solid line) and MAG abundances (dashed line) are separated into total (black), Clade I (blue), Clade IV (red), and Other Clades (green).

Table 1. Genome characteristics of the *Synechococcus* Station P (Syn SP) MAGs.

MAG	Source samples	Clade	Assembled genome size (Mbp)	Completeness (%)	Contamination (%)	#Contigs	GC%
Syn_SP1	0–95 m	IV	1.99	95.29	0.27	116	54.87
Syn_SP2	0–95 m	I	2.21	97.92	1.64	81	53.4

Clade: *Synechococcus* clade MAG binned to within GTDB.

population at all depths, with Clade IV most prevalent at 50 m and Clade I at 70 m.

Assembly of short and long reads produced two high quality *Synechococcus* genomes (Syn-SP1 and Syn-SP2) representing the two dominant clades (Table 1). Syn-SP1 is most closely related to a Single cell Amplified Genome (SAG; *Synechococcus* C sp003208835; 96.5 ANI) collected from 65 m in the subtropical North Pacific and isolates CC9902 and BL107 from *Synechococcus* Clade IV (87.6 and 87.1 ANI respectively) [53]. The second *Synechococcus* MAG (Syn-SP2) is phylogenetically distant from Syn-SP1 (77.6% ANI) and a member of Clade I that is closely related to SAG *Synechococcus*_C sp002500205 (90.9 ANI) and isolates CC9311 and WH8020 (87.9 and 87.6 ANI respectively). Syn-SP1's genome is similar in size to other known Clade IV members (estimated 2.09 Mb at 100% complete, compared to 2.23–2.29 Mb for complete Clade IV genomes), while Syn-SP2's genome is smaller than other Clade I members (estimated 2.26 Mb genome at 100% complete, compared to 2.53–2.70 Mb for complete Clade I genomes) [54].

These MAGs are the first genomes from *Synechococcus* clades known to dominate these high-latitude regions as identified with single gene analysis [19, 52].

Absolute quantification of MAG populations
We estimated the volumetric abundances (genomes L^{-1}) of the *Synechococcus* MAG populations by deriving a coverage-based recovery ratio from the internal standard genome reads. Concentrations of the MAG populations were $3–6 \times 10^6$ genomes L^{-1} at the surface, and $2–4 \times 10^7$ genomes L^{-1} at the DCM (50–70 m) (Fig. 2B). Summed, the two MAGs accounted for nearly all *Synechococcus* genome abundances, as determined by either metagenome-derived *recA* counts (MAGs were 96% of total *Synechococcus recA*) or flow cytometry (97% of *Synechococcus* flow cytometry counts). The Syn-SP1 MAG accounted for an average of 93% of the clade IV population. The Syn-SP2 MAG accounted for an average of 106% of the clade I population. We further validated the dominance of the SP1 and SP2 populations by mapping the
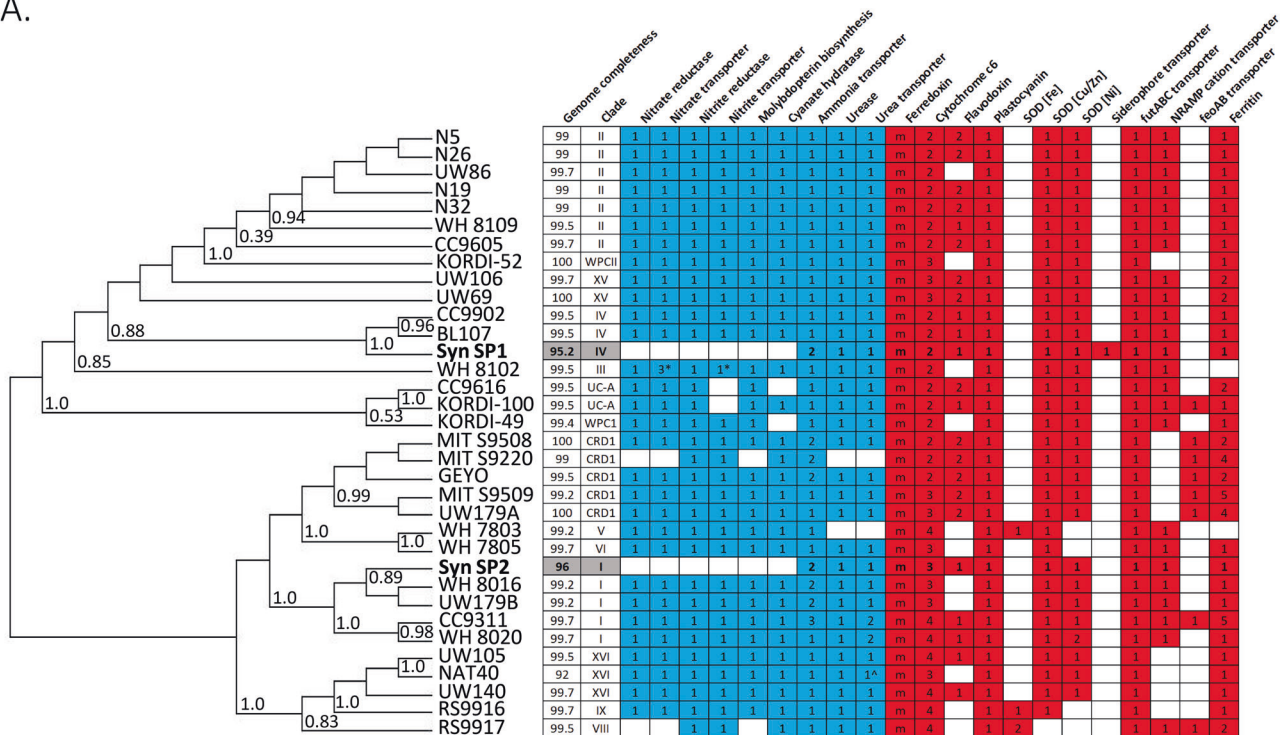
metagenome reads to the MAGS and found 95% of unassembled *Synechococcus* metagenome reads mapped to the two MAGs. The MAGs thus represent the dominant *Synechococcus* populations and their genomic composition at Station P during our sampling.
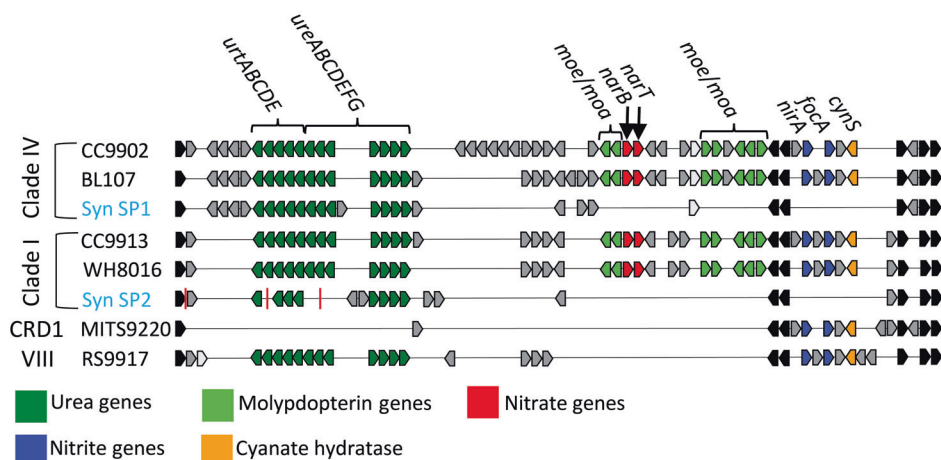
Adaptations of *Synechococcus* MAGs

The Station P *Synechococcus* genomes encode several strategies to cope with low iron availability; strategies that are well distributed across *Synechococcus clades* (Fig. 3A and Supplementary Fig. S3). For iron transport, both genomes possess NRAMP Fe/Mn and *idiABC* iron transporters. In addition, Syn-SP1 contains an operon for importing iron-chelated siderophores. These siderophore transport genes have previously been identified in members of Clades II, III, IV, CRD2, and UC-B, though these genomes were not complete enough to be confidently compared in our analysis of gene presence/absence (Supplementary Fig. S3) [16, 20]. It is unclear whether these populations synthesize their own siderophores or can obtain siderophores released by other community members [55]. Both Station P genomes possess a single copy of the ferritin gene for iron storage and Fur iron regulatory system. Equatorial HNLC-associated *Synechococcus* clade CRD1 possess multiple ferritin genes, potentially as an adaptation to low iron availability [20]. The Station P genomes encode a suite of alternative, low iron-containing proteins for core photosynthesis and electron transport chain functions, in addition to their high-iron dependent counterparts. This includes flavodoxin as a ferredoxin substitute and plastocyanin as a cytochrome c6 substitute, and the presence of only superoxide dismutases

A.

Genome	Genome completeness	Clade	Nitrate reductase	Nitrate transporter	Nitrite reductase	Nitrite transporter	Molybdopterin biosynthesis	Cyanate hydratase	Ammonia transporter	Urease	Urea transporter	ferredoxin	Cytochrome c6	Flavodoxin	Plastocyanin	SOD [Fe]	SOD [Cu/Zn]	SOD [Ni]	Siderophore transporter	futABC transporter	NRAMP cation transporter	feoAB transporter	Ferritin
N5	99	II	1	1	1	1	1	1	1	1	1	m	2	2	1		1	1		1	1		1
N26	99	II	1	1	1	1	1	1	1	1	1	m	2	2	1		1	1		1	1		1
UW86	99.7	II	1	1	1	1	1	1	1	1	1	m	2		1		1	1		1	1		1
N19	99	II	1	1	1	1	1	1	1	1	1	m	2	2	1		1	1		1	1		1
N32	99	II	1	1	1	1	1	1	1	1	1	m	2	2	1		1	1		1	1		1
WH 8109	99.5	II	1	1	1	1	1	1	1	1	1	m	2	1	1		1	1		1	1		1
CC9605	99.7	II	1	1	1	1	1	1	1	1	1	m	2	2	1		1	1		1	1		1
KORDI-52	100	WPCII	1	1	1	1	1	1	1	1	1	m	3		1		1	1		1			1
UW106	99.7	XV	1	1	1	1	1	1	1	1	1	m	3	2	1		1	1		1	1		1
UW69	100	XV	1	1	1	1	1	1	1	1	1	m	3	2	1		1	1		1	1		2
CC9902	99.5	IV	1	1	1	1	1	1	1	1	1	m	2	2	1		1	1		1	1		1
BL107	99.5	IV	1	1	1	1	1	1	1	1	1	m	2	1	1		1	1		1	1		1
Syn SP1	**95.2**	**IV**							2	1	1	m	2	1	1		1	1	1	1	1	1	1
WH 8102	99.5	III	1	3*	1	1*	1	1	1	1	1	m	2		1		1	1		1	1		2
CC9616	99.5	UC-A	1	1	1		1	1	1	1	1	m	2	2	1		1	1		1	1		2
KORDI-100	99.5	UC-A	1	1	1		1	1	1	1	1	m	2		1		1	1		1	1	1	1
KORDI-49	99.4	WPC1	1	1	1		1	1	1	1	1	m	2		1		1	1		1	1		1
MIT S9508	100	CRD1	1	1	1	1	1	1	2	1	1	m	2	2	1		1	1		1	1	2	2
MIT S9220	99	CRD1		1	1		1	1	2			m	2	2	1		1	1		1	1	1	4
GEYO	99.5	CRD1	1	1	1	1	1	1	2	1	1	m	2	2	1		1	1		1	1	2	2
MIT S9509	99.2	CRD1	1	1	1	1	1	1	1	1	1	m	3	2	1		1	1		1	1	1	5
UW179A	100	CRD1	1	1	1	1	1	1	1	1	1	m	3	2	1		1	1		1	1	4	4
WH 7803	99.2	V	1	1	1	1	1	1	1		1	m	4		1	1	1			1	1		1
WH 7805	99.7	VI	1	1	1	1	1	1	1		1	m	3		1		1			1	1		1
Syn SP2	**96**	**I**							2	1	1	m	3	1	1		1	1		1	1	1	1
WH 8016	99.2	I	1	1	1	1	1	1	2	1	1	m	3		1		1	1		1	1		1
UW179B	99.2	I	1	1	1	1	1	1	2	1	1	m	3		1		1	1		1	1		1
CC9311	99.7	I	1	1	1	1	1	1	3	1	2	m	4	1	1		1	1		1	1	1	5
WH 8020	99.7	I	1	1	1	1	1	1	1	1	2	m	4	1	1		1	2		1	1		1
UW105	99.5	XVI	1	1	1	1	1	1	1	1	1	m	4		1		1	1		1	1		1
NAT40	92	XVI	1	1	1	1	1	1	1	1	1^	m	3		1		1	1		1	1		1
UW140	99.7	XVI	1	1	1	1	1	1	1	1	1	m	4	1	1		1	1		1	1		1
RS9916	99.7	IX	1	1	1	1	1	1	1	1	1	m	4		1	1	1			1	1		1
RS9917	99.5	VIII		1	1		1	1	1	1	1	m	4		1		1	2		1	1	1	2

B.

Gene cluster labels: urtABCDE, ureABCDEFG, moe/moa, narB, narT, moe/moa, cynS, focA, nirA

	Genome
Clade IV	CC9902
	BL107
	Syn SP1
Clade I	CC9913
	WH8016
	Syn SP2
CRD1	MITS9220
VIII	RS9917

Legend:
- Urea genes
- Molypdopterin genes
- Nitrate genes
- Nitrite genes
- Cyanate hydratase

Fig. 3 Comparison of marine *Synechococcus* nitrogen and iron utilization strategies. A Phylogenomic distribution of nitrogen acquisition (blue) and selected iron requiring genes (red) across *Synechococcus* clades. Phylogenetic relatedness was determined by multiple sequence alignment of each genome's concatenated 120 bacterial marker genes in GTDB-TK. Station P *Synechococcus* MAGs are bolded and highlighted in gray. Numbers in a column represent gene copies in a genome, with m standing for multiple copies of the ferredoxin gene, and ^ standing for partial presence of the gene pathway. Only genomes with an estimated completeness of >90% are included here (for a complete set of genomes see Supplementary Fig. 3). **B** Distribution of nitrogen assimilation genes across select *Synechococcus* genomes. Station Papa MAGs are labeled in blue. Light gray indicates homologous genes that are present in different order within gene region. Red vertical lines indicate contig breaks.

that use copper and zinc or nickel cofactors instead of iron [56–58]. Overall, the Station P genomes encode multiple strategies for obtaining and conserving iron, but these strategies are not unique to them, rather most of them are broadly distributed in *Synechococcus* genomes obtained from both low and high iron environments.

The Station P *Synechococcus* genomes were unusual in their nitrogen assimilation pathway in that they are the first known *Synechococcus* genomes to be missing the entire nitrate/nitrite reduction pathway. Within a nitrogen gene cluster highly conserved among cyanobacteria, both genomes are missing genes for nitrate reductase, nitrite reductase, nitrate and nitrite transporters, cyanate hydratase, and the nitrate reductase cofactor molybdopterin biosynthesis genes (Fig. 3B). By contrast, the genomes both contain two distinct ammonium transporters, all urease subunits, and a urea ABC transporter. For the two ammonium transporters found in both Syn-SP1 and Syn-SP2, one is closely related to other *Synechococcus* ammonium transporters, and the other is closely related to euryarchaeal and Thermotogae ammonium transporters (Supplementary Fig S4). Both of these ammonium transporter types are present in closely related *Synechococcus* genomes that contain two ammonium transporters.

Support for the absence of nitrate and nitrite utilization genes from Station P *Synechococcus* populations is provided by (1) the high quality and completeness of the MAGs from multiple independent assemblies, (2) the missing nitrogen genes' location in the interior of a contig flanked by nitrogen genes with homology to taxonomically related genomes, and (3) individual long Nanopore reads lacking these genes (Supplementary Fig. S5).

To further increase confidence that nitrate and nitrite assimilation genes are absent in Station P *Synechococcus* populations, we determined *Synechococcus* nitrogen gene copy numbers in the unassembled metagenomes. If the majority of Station P *Synechococcus* genomes possess nitrate reductase (narB), then narB copies per genome should be approximately one (Fig. 4). Instead, we found *Synechococcus* narB copy numbers much less than one (range 0.04–0.26), supporting their depletion in Station P *Synechococcus* populations, with the nitrate reductase genes present mostly belonging to Clade IV. Nitrite reductase (nirA) gene ratios were higher (range 0.42–1.35), though this may be due to misannotation given nirA's high sequence similarity to sulfite reductase. Copy numbers for the nitrate transporter narT and the

nitrite/formate transporter focA were also much lower than one, supporting depletion in the Station P *Synechococcus* populations. focA gene abundance was approximately 25% for the *Synechococcus* community, with nitrite transporters from both Clades I and IV, so it is likely that at least two *Synechococcus* variants with nitrite reductase represent a fraction of the station P population. Based on this data, it appears that, though the Synechococcus backbone represented by our Syn-SP1 and SP2 genomes represent ~97% of the Synechococcus population, at least a few other ecotypes sharing this backbone are present within this community that contain a whole or partial nitrate reduction pathway and represent up to a quarter of the total Synechococcus population at Station P. These other ecotypes may be present at higher abundances during other seasons, such as during the small spring phytoplankton bloom that occurs at Station P. By contrast, *Synechococcus* ammonium transporter (amt) genome copy numbers were between two and three across all Station P samples (range 0.91–2.77), consistent with the two amt copies in our *Synechococcus* genomes.

The Station P genomes are the first known *Synechococcus* to lack both nitrate and nitrite uptake and utilization genes. Two previously sequenced *Synechococcus* genomes do not encode the ability to use nitrate but are capable of nitrite assimilation: MIT S9220 isolated from an HNLC zone in the Equatorial Pacific, and RS9917 isolated from the Red Sea [59–61]. Both isolates were obtained using media with ammonium as the nitrogen source. The loss of both nitrate and nitrite assimilation therefore may be specific to high latitude HNLC *Synechococcus*, though more metagenome sequencing and cultivation on non-traditional *Synechococcus* media (with ammonium used as N source instead of traditionally used nitrate) is needed [62, 63].

The absence of nitrate and nitrite assimilation and the enrichment of ammonium transporters suggests the dominant *Synechococcus* populations at Station P cannot utilize nitrate or nitrite as a nitrogen source and instead rely on ammonium or other reduced forms of recycled nitrogen for growth. Despite high concentrations of nitrate in this region, the benefit to losing nitrate and nitrite assimilation is a decreased cellular iron and energy demand. Reduction of exogenous nitrate and nitrite to ammonium requires a large quantity of iron, with nitrate reductase containing four iron atoms per enzyme and nitrite reductase containing five iron atoms [11, 64]. In many areas of the ocean, iron stress is coupled with nitrogen stress leading cyanobacteria to maintain assimilation capabilities for all sources of N, including nitrate and nitrite, and their associated high iron cost [65]. However, in HNLC regions such as Station P, abundant N sources, particularly ammonium and urea, may drive the system more heavily towards iron limitation, resulting in evolutionary pressure to prioritize iron conservation over nitrate utilization via loss of the nitrate/nitrite assimilation pathway [66].

Global patterns in nitrate and nitrite assimilation loss

To examine whether *Synechococcus* nitrate and nitrite assimilation loss is widespread in the global ocean, we extended the nitrogen gene copy number analysis to the TARA Oceans metagenomes. TARA Oceans metagenomes from the 0.2–3.0 μm size fraction were annotated via BLASTX searches to identify *Synechococcus* nitrate reductase (narB), nitrite transporter (focA), ammonium transporter (amt), and recombinase A (recA) gene hits in order to calculate nitrogen gene copy numbers per genome equivalents across the global ocean. The ratios at each station were then compared to surface nitrate and dissolved iron concentrations (N:Fe ratios, or nanomolar nitrate divided by nanomolar iron) predicted by the PISCES global ocean biogeochemical model [67, 68]. Station P *Synechococcus* narB and focA genome copies were depleted compared to most TARA stations (Fig. 5A). By contrast, *Synechococcus* ammonium transporters (amt) were typically found at greater than one copy per genome at both
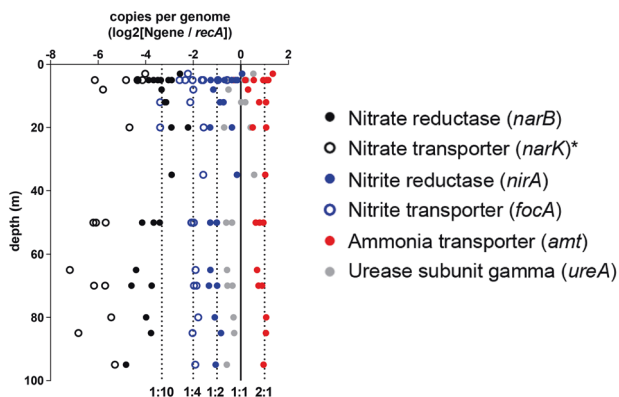
Fig. 4   Depth distribution of nitrogen assimilation gene prevalence in Station P unassembled metagenomes. Nitrogen gene copy numbers per genome were calculated as the ratio of *Synechococcus* nitrogen gene read abundance to *Synechococcus* recA read abundance, and then log2 normalized. The solid vertical line is the 1:1 ratio representing a single copy of the gene per recA (*Synechococcus* genome equivalent), with dotted lines representing other genome copy numbers. *Seven samples are not included due to no nitrate transporter reads found in those samples.
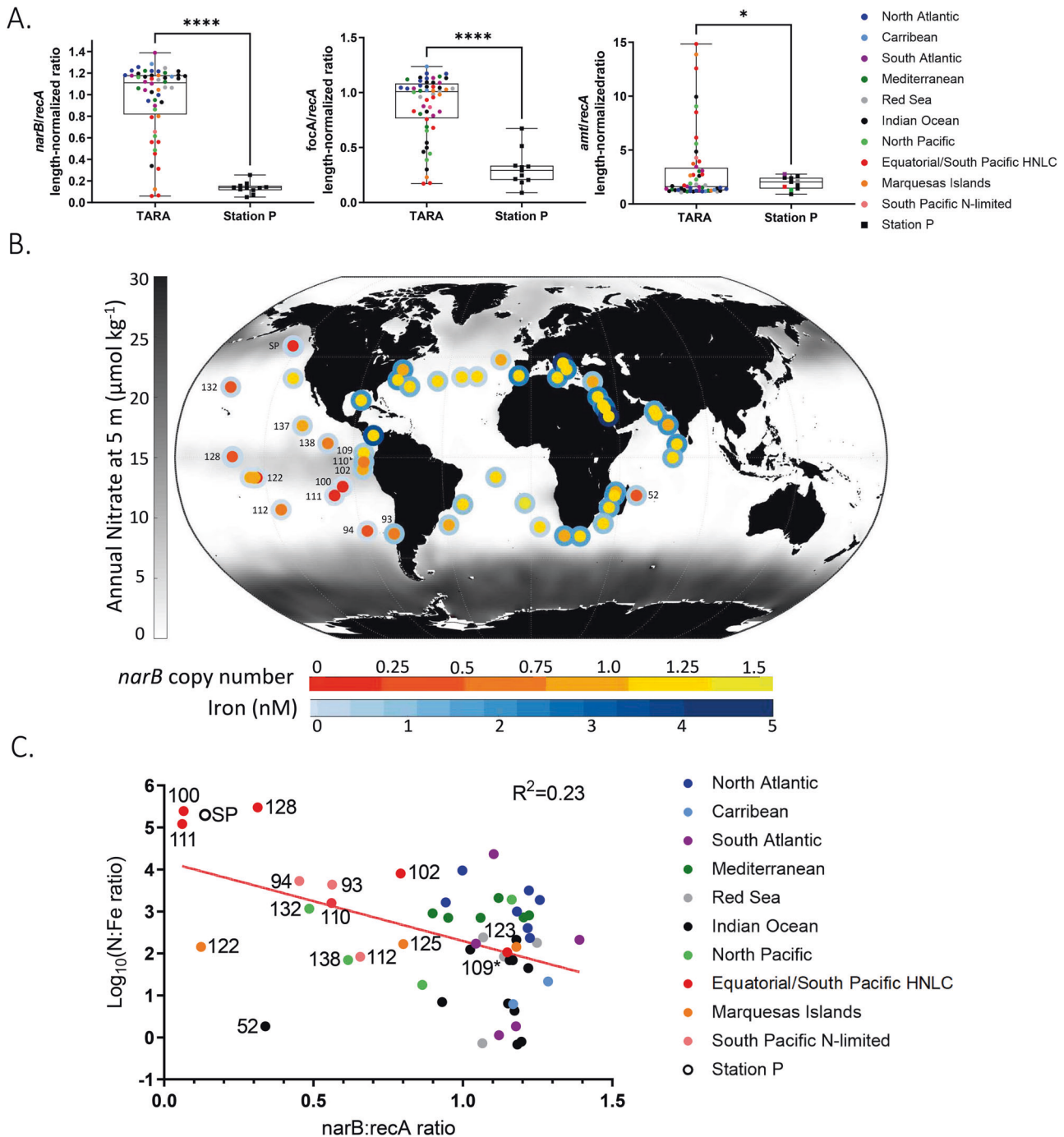
Fig. 5 Global prevalence of *Synechococcus* select nitrogen metabolism genes in relation to iron and nitrogen standing stocks. **A** *Synechococcus g*ene copy numbers for nitrate reductase, nitrite/formate transporter, and ammonium transporters for all TARA Stations and all EXPORTS Station P samples at 5 m depth. Significance of *p*-value of Welch's t test signified by *($p < 0.05$) and ****($p < 0.0001$). **B** Global patterns of nitrate (background map), dissolved iron concentrations (outer circle of each datapoint), and *Synechococcus* nitrate reductase genome copy numbers (inner circle of each datapoint) for TARA stations and Station P (SP). *Synechococcus* nitrogen copy numbers were calculated using gene length normalized ratios derived from the TARA dataset. Annually averaged nitrate concentrations (μmol kg^{-1}) were derived from the WOA2018 global dataset. Dissolved iron concentrations (nM) determined from the PISCES biogeochemical model and BYONIC 3 R biogeochemistry dataset. **C** Log$_{10}$ normalized nitrate to iron ratio versus *Synechococcus* nitrate reductase gene copy number of the TARA stations and EXPORTS Station P. Red line indicates the linear regression ($R^2 = 0.23$, *p*-value $= 0.0004$). Select stations within the Pacific and Indian Oceans are labeled with their TARA ID.

Station P and TARA stations, though there was a statistically significant enrichment at Station P (Fig. 5A).

Based on the TARA metagenome and PISCES nutrient data, nitrate reductase (*narB*) copy numbers are low in the HNLC regions of the southeastern and equatorial Pacific that have high nitrate and low chlorophyll *a* concentrations (Fig. 5B, C; linear regression, $p < 0.05$, $R^2 = 0.23$). Similar to Station P, HNLC zones also have low nitrite transporter (*focA*) and high ammonium transporter (*amt*) copy numbers (Supplementary Fig. S6A). Additionally, principal component analysis (PCA) was used with the

three nitrogen gene copy numbers and the N:Fe ratios as variables. The PCA analysis showed that Station P clusters with Station 128, the most isolated Equatorial Pacific HNLC Tara Station, while other HNLC stations clustered away from the majority of other TARA Stations Supplementary Fig. S6B). Two outliers, Station 52 (Southwest Indian Ocean) and Station 122 (East of Marquesas Islands), also had low *narB* copy numbers despite having low predicted annual N:Fe ratios. However, modeled nutrient profiles of these two regions suggest they are iron-limited for large parts of the year, with iron inputs occurring seasonally, and thus the annual modeled N:FE ratio may be too broad to capture the complexity of nutrient limitation at these sites [69, 70]. Aside from these outliers, the lowest *narB* copy numbers correspond with Station P and the TARA Stations with the highest N:Fe ratios, all of which are within or adjacent to HNLC regions, supporting nitrate assimilation gene loss is linked to iron limitation (Fig. 5C).

SYNTHESIS
Our findings suggest the dominant *Synechococcus* at Station P are likely incapable of assimilating either nitrate or nitrite and instead rely on reduced nitrogen sources such as ammonium and urea. Traditionally, nitrate and nitrite assimilation has been considered to be a core trait of *Synechococcus*, as they are known to possess the entire nitrate assimilation pathway and exhibit cellular heterogeneity of nitrate uptake as an adaptation to fluctuating nitrate availability [71]. However, in iron-limited HNLC zones, these genes may be less advantageous, with the loss of genes for nitrate and/or nitrite assimilation eliminating the cellular iron demand required by their respective reductases. The f-ratios were low at Station P, particularly in small cells below the mixed layer where *Synechococcus* is most abundant, which could be attributed in part to the lack of *Synechococcus* nitrate and nitrite uptake capabilities.

The TARA Oceans nitrogen gene analysis indicates *Synechococcus* nitrate reductases are also depleted within the equatorial and sub-tropical Southern Pacific HNLC regions as well as in a portion of the Southwestern Indian Ocean, with nitrite transporters also being as depleted as Station P in the most isolated portion of the equatorial Pacific HNLC zone (TARA Station 128). Conversely, ammonium transporters are enriched in Pacific HNLC zones and at Station P. The results suggest having both nitrate and nitrite assimilation capabilities, or nitrite assimilation alone, is not a core trait of marine *Synechococcus*. Isolation of these HNLC Synechococcus and in vivo investigations of their iron quotas and growth on various nitrogen compounds is necessary to confirm this hypothesis [59–61].

These new *Synechococcus* genomes display signs of genomic streamlining and iron-scavenging strategies that may aid their survival in the iron-limited environment at Station P. *Synechococcus sp.* SP1 has an estimated 6% smaller genome compared to close Clade IV relatives, while SP2 has an estimated 13% reduction in genome size compared to its Clade I relatives. The smaller genomes reduce the overall nitrogen and phosphorus requirements for genome maintenance and replication, which could be an important means of reducing macronutrient quotas when iron limitation prevents their uptake and utilization. *Synechococcus sp.* SP1 also possesses a putative siderophore uptake system, while SP2 does not appear to possess one. Interestingly, unlike recently identified siderophore-possessing *Prochlorococcus*, which tend to be low light and low temperature adapted strains (HLI and LLI ecotypes) that reside primarily at the deepest chlorophyll maximums, SP1 at Station P has siderophore uptake and resides at the surface as well as down to 70 m. Meanwhile, the more deepwater associated SP2 lives at 50–85 m with no detected siderophore uptake system [16]. This difference in vertical organization of siderophore uptake gene presence might be due to the difference in the dissolved iron depth profile, with iron concentrations being depleted at the surface and increasing with depth where SP2 is most abundant, forgoing the need for siderophore uptake by this strain.

The disparate loss of nitrogen assimilation genes across the *Synechococcus* phylogeny suggests multiple factors might be influencing their retention. If iron limitation exerts a significant selective pressure for nitrogen gene loss, whether that be directly as an iron-limitation strategy or indirectly due to iron-limitation causing the buildup of reduced nitrogen that forgoes the need for nitrate assimilation, why have high latitude HNLC *Synechococcus* lost both nitrate and nitrite assimilation while equatorial HNLC *Synechococcus* strains only abandon a portion of the pathway? This may be due to dueling pressures between iron stress and competition for reduced nitrogen species. Complete loss of nitrate and nitrite assimilation may only be possible at high latitudes where there is reduced competition for ammonium from other cyanobacteria. *Prochlorococcus* is a major competitor for reduced nitrogen species, often relying solely on ammonium as their nitrogen source. They are dominant in many low to mid latitude regions but absent at high latitudes [3, 6, 11, 72], including Station P where they are undetectable by pigment analysis, flow cytometry, and metagenomics. In low latitude HNLC regions, competition with *Prochlorococcus* and heterotrophic bacteria may result in *Synechococcus* at least maintaining nitrite uptake. In high latitude HNLC regions, competition for ammonium is lower due to the absence of *Prochlorococcus*. Further, overall community competition for ammonium is likely low at Station P given the relatively high standing stocks of ammonium at the DCM; Station P's peak ammonium concentration was greater than threefold higher than those measured in equatorial HNLC sites (Supplementary Fig. S7).

The model for *Prochlorococcus* nitrogen gene gain and loss appears to be a close counterpart to *Synechococcus*, where nitrogen gene retention is selected for by nitrogen competition but selected against in iron- or light-limiting environments [11, 73]. Low-light *Prochlorococcus* typically possess only nitrite assimilation genes and are abundant at the subsurface nitrite maximum at the base of the euphotic zone [72]. Competition for ammonium near the nitrite maximum is intense due to the presence of ammonia-oxidizing archaea, driving low-light *Prochlorococcus* to acquire nitrite generated by ammonia oxidizers [74–76]. Additionally, most low-light *Prochlorococcus* are restricted to the base of the euphotic zone, where the energy required to reduce nitrate may drive selection against maintaining nitrate assimilation [11, 72]. High-light *Prochlorococcus* suffer less light limitation and many strains possess both nitrate and nitrite assimilation pathways [6, 11, 77]. Critically, high-light *Prochlorococcus* clades adapted to low-iron conditions in the Equatorial Pacific HNLC zone do not contain nitrate and nitrite utilization genes, reducing their iron requirements [11, 18, 78].

The reduced ability to assimilate nitrate and nitrite by some *Synechococcus* populations suggests a re-evaluation of their role in HNLC nutrient cycles and carbon export. In these regions, iron availability limits primary production and nitrate utilization due to the iron requirements for their respective enzymes. New iron delivered to this region via lateral advection, entrainment from subsurface waters, or from atmospheric inputs leads to pulses of nitrate-based new production typically dominated by large phytoplankton (i.e., diatoms) that exceed surface remineralization and can be exported [79]. However, according to our findings, any new inputs of iron would not stimulate nitrate utilization and subsequent nitrate-fueled growth in the dominant *Synechococcus* population at Station P, prohibiting them from significantly contributing to organic carbon export fluxes. Instead, these Station P *Synechococcus* strains are confined to a tight recycling loop where they are dependent on other primary producers to assimilate nitrate, which then directly or indirectly regulates the subsequent availability of recycled forms of nitrogen such as ammonium or urea. The direct inability of these *Synechococcus*

strains to contribute to new production means their fixed carbon is continuously cycled in the surface ocean when grazed upon or remineralized by bacterioplankton, leaving little carbon to be exported to depth. Thus, whereas small cyanobacteria such as *Prochlorococcus* and *Synechococcus* can be major contributors to ocean carbon export, in the North Pacific and possibly other HNLC regions, this may not always be the case [1, 6, 80, 81].

It should be noted that these strains may not dominate the *Synechococcus* community at Station P throughout the year. While our analysis suggests the dominant *Synechococcus* populations at Station P do not contain nitrate and nitrite assimilation pathways, we did detect the presence of these genes at relatively low levels (<10% of genome equivalents for *narB*, and ~29% of genome equivalents for *focA*) in the unassembled metagenome. This suggests there is a small population of nitrate/nitrite and nitrite utilizing *Synechococcus* ecotypes maintained in the community. At different times of the year these populations may increase in abundance, potentially when iron is pulsed into the system, altering nitrogen cycles and carbon export potential by the *Synechococcus* community at Station P. Alternatively, these nitrate/ nitrite utilizing ecotypes could persist at lower abundance year round and compensate for the increased iron quota of these genes through some other iron conservation strategies, such as iron storage, iron uptake, or transcriptional controls on their nitrogen assimilation machinery. This emphasizes the need for further genomic and biogeochemical investigations to model the role of cyanobacteria more accurately in the Fe, N, and C cycles of HNLC zones. Further, if nitrogen assimilation adaptation driven by iron limitation is prevalent within other HNLC *Synechococcus* populations, as our TARA Oceans analysis suggests, it has significant impacts on nutrient cycling and associated carbon export by the cyanobacterial community in a sizable fraction of the global ocean. Overall, our results further support how iron availability affects primary productivity directly through limitation but also has fundamentally shaped phytoplankton functional capabilities leading to cascading effects on marine biogeochemical cycles and food webs.

DATA AVAILABILITY
All metagenomes have been submitted to NCBI under BioProject PRJNA785333 (Biosamples SAMN24695624-SAMN24695646.)

REFERENCES
1. Richardson TL, Jackson GA. Small phytoplankton and carbon export from the surface ocean. Science. 2007;315:838–40.
2. Flombaum P, Gallegos JL, Gordillo RA, Rincón J, Zabala LL, Jiao N, et al. Present and future global distributions of the marine Cyanobacteria Prochlorococcus and Synechococcus. Proc Natl Acad Sci USA. 2013;110:9824–9.
3. Johnson ZI, Zinser ER, Coe A, McNulty NP, Woodward EMS, Chisholm SW. Niche partitioning among Prochlorococcus ecotypes along ocean-scale environmental gradients. Science. 2006;311:1737–40.
4. Sohm JA, Capone DG. Phosphorus dynamics of the tropical and subtropical north Atlantic: Trichodesmium spp. versus bulk plankton. Mar Ecol Prog Ser. 2006;317:21–8.
5. Ahlgren NA, Rocap G. Diversity and distribution of marine synechococcus: multiple gene phylogenies for consensus classification and development of qPCR assays for sensitive measurement of clades in the ocean. Front Microbiol. 2012;3:213.
6. Martiny AC, Kathuria S, Berube PM. Widespread metabolic potential for nitrite and nitrate assimilation among Prochlorococcus ecotypes. Proc Natl Acad Sci USA. 2009;106:10787–92.
7. Raven JA, Evans MCW, Korb RE. The role of trace metals in photosynthetic electron transport in O2-evolving organisms. Photosynth Res. 1999;60:111–50.
8. Morrissey J, Bowler C. Iron utilization in marine cyanobacteria and eukaryotic algae. Front Microbiol. 2012;3:43.
9. Raven JA. The iron and molybdenum use efficiencies of plant growth with different energy, carbon and nitrogen sources. New Phytol. 1988;109:279–87.
10. Morel FMM, Price NM. The biogeochemical cycles of trace metals in the oceans. Science. 2003;300:944–7.
11. Berube PM, Rasmussen A, Braakman R, Stepanauskas R, Chisholm SW. Emergence of trait variability through the lens of nitrogen assimilation in Prochlorococcus. Elife. 2019;8:e41043.
12. Boyd PW, Ellwood MJ. The biogeochemical cycle of iron in the ocean. Nat Geosci. 2010;3:675–82.
13. Martin JH, Gordon RM, Fitzwater S, Broenkow WW. Vertex: phytoplankton/iron studies in the Gulf of Alaska. Deep Sea Res A. 1989;36:649–80.
14. Moore JK, Doney SC, Glover DM, Fung IY. Iron cycling and nutrient-limitation patterns in surface waters of the World Ocean. Deep Sea Res Part 2 Top Stud Oceanogr. 2001;49:463–507.
15. Thompson AW, Huang K, Saito MA, Chisholm SW. Transcriptome response of high- and low-light-adapted Prochlorococcus strains to changing iron availability. ISME J. 2011;5:1580–94.
16. Hogle SL, Hackl T, Bundy RM, Park J, Satinsky B, Hiltunen T, et al. Siderophores as an iron source for picocyanobacteria in deep chlorophyll maximum layers of the oligotrophic ocean. ISME J. 2022;16:1636–46.
17. Mackey KRM, Post AF, McIlvin MR, Cutter GA, John SG, Saito MA. Divergent responses of Atlantic coastal and oceanic Synechococcus to iron limitation. Proc Natl Acad Sci USA. 2015;112:9944–9.
18. Rusch DB, Martiny AC, Dupont CL, Halpern AL, Venter JC. Characterization of Prochlorococcus clades from iron-depleted oceanic regions. Proc Natl Acad Sci USA. 2010;107:16184–9.
19. Ahlgren NA, Belisle BS, Lee MD. Genomic mosaicism underlies the adaptation of marine Synechococcus ecotypes to distinct oceanic iron niches. Environ Microbiol. 2020;22:1801–15.
20. Sohm JA, Ahlgren NA, Thomson ZJ, Williams C, Moffett JW, Saito MA, et al. Co-occurring Synechococcus ecotypes occupy four major oceanic regimes defined by temperature, macronutrients and iron. ISME J. 2016;10:333–45.
21. Mühling M, Fuller NJ, Somerfield PJ, Post AF, Wilson WH, Scanlan DJ, et al. High resolution genetic diversity studies of marine Synechococcus isolates using rpoC1-based restriction fragment length polymorphism. Aquat Microb Ecol. 2006;45:263–75.
22. Xia X, Cheung S, Endo H, Suzuki K, Liu H. Latitudinal and vertical variation of synechococcus assemblage composition along 170° W transect from the South Pacific to the Arctic Ocean. Microb Ecol. 2019;77:333–42.
23. Farrant GK, Doré H, Cornejo-Castillo FM, Partensky F, Ratin M, Ostrowski M, et al. Delineating ecologically significant taxonomic units from global patterns of marine picocyanobacteria. Proc Natl Acad Sci USA. 2016;113:E3365–74.
24. Siegel DA, Cetinić I, Graff JR, Lee CM, Nelson N, Perry MJ, et al. An operational overview of the EXport Processes in the Ocean from RemoTe Sensing (EXPORTS) Northeast Pacific field deployment. Vol. 9, Elem Sci Anth. 2021. p. 00107.
25. Graff JR, Behrenfeld MJ. Photoacclimation responses in subarctic atlantic phytoplankton following a natural mixing-restratification event. Front Marine Sci. 2018;5. p. 1–11.
26. Meyer MG, Gong W, Kafrissen SM, Torano O, Varela DE, Santoro AE, et al. Phytoplankton size-class contributions to new and regenerated production during the EXPORTS Northeast Pacific Ocean field deployment. Elem Sci Anth. 2022;10:00068.
27. Buchfink B, Xie C, Huson DH. Fast and sensitive protein alignment using DIAMOND. Nat Methods. 2015;12:59–60.
28. Nurk S, Meleshko D, Korobeynikov A, Pevzner PA. metaSPAdes: a new versatile metagenomic assembler. Genome Res. 2017;27:824–34.
29. Langmead B, Salzberg SL. Fast gapped-read alignment with Bowtie 2. Nat Methods. 2012;9:357–9.
30. Li H, Handsaker B, Wysoker A, Fennell T, Ruan J, Homer N, et al. The sequence alignment/map format and SAMtools. Bioinformatics. 2009;25:2078–9.
31. Kang DD, Li F, Kirton E, Thomas A, Egan R, An H, et al. MetaBAT 2: an adaptive binning algorithm for robust and efficient genome reconstruction from metagenome assemblies. PeerJ. 2019;7:e7359.
32. Wu Y-W, Tang Y-H, Tringe SG, Simmons BA, Singer SW. MaxBin: an automated binning method to recover individual genomes from metagenomes using an expectation-maximization algorithm. Microbiome. 2014;2:26.
33. Alneberg J, Bjarnason BS, de Bruijn I, Schirmer M, Quick J, Ijaz UZ, et al. CONCOCT: clustering cONtigs on COverage and CompoSiTion. arXiv. 2013. Available from: http://arxiv.org/abs/1312.4038.
34. Sieber CMK, Probst AJ, Sharrar A, Thomas BC, Hess M, Tringe SG, et al. Recovery of genomes from metagenomes via a dereplication, aggregation and scoring strategy. Nat Microbiol. 2018;3:836–43.
35. Parks DH, Imelfort M, Skennerton CT, Hugenholtz P, Tyson GW. CheckM: assessing the quality of microbial genomes recovered from isolates, single cells, and metagenomes. Genome Res. 2015;25:1043–55.
36. Gifford SM, Zhao L, Stemple B, DeLong K, Medeiros PM, Seim H, et al. Microbial niche diversification in the galápagos archipelago and its response to El Niño. Front Microbiol. 2020;11:575194.
37. Satinsky BM, Gifford SM, Crump BC, Moran MA. Use of internal standards for quantitative metatranscriptome and metagenome analysis. Methods Enzymol. 2013;531:237–50. 33

G. Sharpe et al.

10

38. Whitney FA. Nutrient variability in the mixed layer of the subarctic Pacific Ocean, 1987–2010. J Oceanogr. 2011;67:481–92.
39. Nishioka J, Obata H. Dissolved iron distribution in the western and central subarctic Pacific: HNLC water formation and biogeochemical processes. Limnol Oceanogr. 2017;62:2004–22.
40. Boyd P, Harrison PJ. Phytoplankton dynamics in the NE subarctic Pacific. Deep Sea Res Part 2 Top Stud Oceanogr. 1999;46:2405–32. Nov
41. McNair HM, Meyer MG, Lerch SJ, Maas AE, Stephens BM, Fox J, et al. Quantitative analysis of food web dynamics in a low export ecosystem. bioRxiv. 2023. https://www.biorxiv.org/content/10.1101/2023.03.17.532807v1.
42. Hamme RC, Webley PW, Crawford WR, Whitney FA, DeGrandpre MD, Emerson SR, et al. Volcanic ash fuels anomalous plankton bloom in subarctic northeast Pacific. Geophys Res Lett. 2010;37. p. 1–5.
43. Xiu P, Palacz AP, Chai F, Roy EG, Wells ML. Iron flux induced by Haida eddies in the Gulf of Alaska. Geophys Res Lett. 2011;38. p1–5.
44. Fitzsimmons JN, Hayes CT, Al-Subiai SN, Zhang R, Morton PL, Weisend RE, et al. Daily to decadal variability of size-fractionated iron and iron-binding ligands at the Hawaii Ocean Time-series Station ALOHA. Geochim Cosmochim Acta. 2015;171:303–24.
45. Gifford SM, Sharma S, Rinta-Kanto JM, Moran MA. Quantitative analysis of a deeply sequenced marine microbial metatranscriptome. ISME J. 2011;5:461–72.
46. Gifford SM, Becker JW, Sosa OA, Repeta DJ, DeLong EF. Quantitative transcriptomics reveals the growth- and nutrient-dependent response of a streamlined marine methylotroph to methanol and naturally occurring dissolved organic matter. MBio. 2016;7:e01279–16.
47. Satinsky BM, Crump BC, Smith CB, Sharma S, Zielinski BL, Doherty M, et al. Microspatial gene expression patterns in the Amazon River Plume. Proc Natl Acad Sci USA. 2014;111:11085–90.
48. Satinsky BM, Smith CB, Sharma S, Landa M, Medeiros PM, Coles VJ, et al. Expression patterns of elemental cycling genes in the Amazon River Plume. ISME J. 2017;11:1852–64.
49. Lin Y, Gifford S, Ducklow H, Schofield O, Cassar N. Towards quantitative microbiome community profiling using internal standards. Appl Environ Microbiol. 2019;85:e02634–18.
50. Crossette E, Gumm J, Langenfeld K, Raskin L, Duhaime M, Wigginton K. Metagenomic quantification of genes with internal standards. MBio. 2021;12:e03173–20.
51. Zwirglmaier K, Jardillier L, Ostrowski M, Mazard S, Garczarek L, Vaulot D, et al. Global phylogeography of marine Synechococcus and Prochlorococcus reveals a distinct partitioning of lineages among oceanic biomes. Environ Microbiol. 2008;10:147–61.
52. Paulsen ML, Doré H, Garczarek L, Seuthe L, Müller O, Sandaa R-A, et al. Synechococcus in the Atlantic Gateway to the Arctic Ocean. Front Marine Sci. 2016;3. p. 1–14.
53. Berube PM, Biller SJ, Hackl T, Hogle SL, Satinsky BM, Becker JW, et al. Single cell genomes of Prochlorococcus, Synechococcus, and sympatric microbes from diverse marine environments. Sci Data. 2018;5:180154.
54. Lee MD, Ahlgren NA, Kling JD, Walworth NG, Rocap G, Saito MA, et al. Marine Synechococcus isolates representing globally abundant genomic lineages demonstrate a unique evolutionary path of genome reduction without a decrease in GC content. Environ Microbiol. 2019;21:1677–86.
55. Morris JJ, Lenski RE, Zinser ER. The Black Queen Hypothesis: evolution of dependencies through adaptive gene loss. MBio. 2012;3. https://doi.org/10.1128/mBio.00036-12.
56. Erdner DL, Price NM, Doucette GJ, Peleato ML, Anderson DM. Characterization of ferredoxin and flavodoxin as markers of iron limitation in marine phytoplankton. Mar Ecol Prog Ser. 1999;184:43–53.
57. Frazão C, Soares CM, Carrondo MA, Pohl E, Dauter Z, Wilson KS, et al. Ab initio determination of the crystal structure of cytochrome c6 and comparison with plastocyanin. Structure. 1995;3:1159–69.
58. Sheng Y, Abreu IA, Cabelli DE, Maroney MJ, Miller A-F, Teixeira M, et al. Superoxide dismutases and superoxide reductases. Chem Rev. 2014;114:3854–918.
59. Moore LR, Post AF, Rocap G, Chisholm SW. Utilization of different nitrogen sources by the marine cyanobacteria ProchlorococcusandSynechococcus. Limnol Oceanogr. 2002;47:989–96.
60. Belisle BS, Avila Paz AA, Carpenter AR, Cormier TC, Lewis AJ, Menin LS, et al. Genome sequences of Synechococcus sp. Strain MIT S9220 and cocultured cyanophage SynMITS9220M01. Microbiol Resour Announc. 2020;9:e00481–20.
61. Fuller NJ, Marie D, Partensky F, Vaulot D, Post AF, Scanlan DJ. Clade-specific 16S ribosomal DNA oligonucleotides reveal the predominance of a single marine Synechococcus clade throughout a stratified water column in the Red Sea. Appl Environ Microbiol. 2003;69:2430–43.
62. Waterbury JB. The cyanobacteria—isolation, purification and identification. Prokaryotes. 2006;4:1053–73.
63. Ahlgren NA, Rocap G. Culture isolation and culture-independent clone libraries reveal new marine Synechococcus ecotypes with distinctive light and N physiologies. Appl Environ Microbiol. 2006;72:7193–204.
64. Dose MM, Hirasawa M, Kleis-SanFrancisco S, Lew EL, Knaff DB. The ferredoxin-binding site of ferredoxin: Nitrite oxidoreductase. Differential chemical modification of the free enzyme and its complex with ferredoxin. Plant Physiol. 1997;114:1047–53.
65. Saito MA, McIlvin MR, Moran DM, Goepfert TJ, DiTullio GR, Post AF, et al. Multiple nutrient stresses at intersecting Pacific Ocean biomes detected by protein biomarkers. Science. 2014;345:1173–7.
66. Harrison PJ. Station papa time series: insights into ecosystem dynamics. J Oceanogr. 2002;58:259–64.
67. Richon C, Tagliabue A. Biogeochemical feedbacks associated with the response of micronutrient recycling by zooplankton to climate change. Glob Chang Biol. 2021;27:4758–70.
68. Shaked Y, Twining BS, Tagliabue A, Maldonado MT. Probing the bioavailability of dissolved iron to marine eukaryotic phytoplankton using in situ single cell iron quotas. Global Biogeochem Cycles. 2021;35:e2021GB006979.
69. Raapoto H, Martinez E, Petrenko A, Doglioli A, Gorgues T, Sauzède R, et al. Role of iron in the Marquesas island mass effect. J Geophys Res C Oceans. 2019;124:7781–96.
70. Wiggert JD, Murtugudde RG, Christian JR. Annual ecosystem variability in the tropical Indian Ocean: results of a coupled bio-physical ocean general circulation model. Deep Sea Res Part 2 Top Stud Oceanogr. 2006;53:644–76.
71. Berthelot H, Duhamel S, L'Helguen S, Maguer J-F, Wang S, Cetinić I, et al. NanoSIMS single cell analyses reveal the contrasting nitrogen sources for small phytoplankton. ISME J. 2019;13:651–62.
72. Berube PM, Biller SJ, Kent AG, Berta-Thompson JW, Roggensack SE, Roache-Johnson KH, et al. Physiology and evolution of nitrate acquisition in Prochlorococcus. ISME J. 2015;9:1195–207.
73. Ustick LJ, Larkin AA, Garcia CA, Garcia NS, Brock ML, Lee JA, et al. Metagenomic analysis reveals global-scale patterns of ocean nutrient limitation. Science. 2021;372:287–91.
74. Berube PM, Coe A, Roggensack SE, Chisholm SW. Temporal dynamics of Prochlorococcus cells with the potential for nitrate assimilation in the subtropical Atlantic and Pacific oceans. Limnol Oceanogr. 2016;61:482–95.
75. Lomas MW, Lipschultz F. Forming the primary nitrite maximum: nitrifiers or phytoplankton? Limnol Oceanogr. 2006;51:2453–67.
76. Martens-Habbena W, Qin W, Horak REA, Urakawa H, Schauer AJ, Moffett JW, et al. The production of nitric oxide by marine ammonia-oxidizing archaea and inhibition of archaeal ammonia oxidation by a nitric oxide scavenger. Environ Microbiol. 2015;17:2261–74.
77. Malmstrom RR, Coe A, Kettler GC, Martiny AC, Frias-Lopez J, Zinser ER, et al. Temporal dynamics of Prochlorococcus ecotypes in the Atlantic and Pacific oceans. ISME J. 2010;4:1252–64.
78. Malmstrom RR, Rodrigue S, Huang KH, Kelly L, Kern SE, Thompson A, et al. Ecology of uncultured Prochlorococcus clades revealed through single-cell genomics and biogeographic analysis. ISME J. 2013;7:184–98.
79. Pollard RT, Salter I, Sanders RJ, Lucas MI, Moore CM, Mills RA, et al. Southern Ocean deep-water carbon export enhanced by natural iron fertilization. Nature. 2009;457:577–80.
80. Casey JR, Lomas MW, Mandecki J, Walker DE. Prochlorococcus contributes to new production in the Sargasso Sea deep chlorophyll maximum. Geophys Res Lett. 2007;34. p. 1–5.
81. Guidi L, Chaffron S, Bittner L, Eveillard D, Larhlimi A, Roux S, et al. Plankton networks driving carbon export in the oligotrophic ocean. Nature. 2016;532:465–70.

ACKNOWLEDGEMENTS
We are grateful to the NASA EXPORTS project leaders David Siegel (UCSB) and Ivona Cetinić (NASA), chief scientist Deborah Steinberg (VIMS), the captain and crew of the *R/V Roger Revelle*, and all the members of the EXPORTs team. We thank Matt Kellom for Amt alignments and analysis, as well as Nicolas Cassar and Alex Niebergall for global map figure creation. This research was supported by NASA grant 80NSSC17K0552 to SG, AM, and NC, NASA award 80NSSC18K1431 to AS, NASA award 80NSSC17K0568 to Michael J. Behrenfeld (Co-I J.R. Graff), and NSF award OCE-1756433 to KNB.

AUTHOR CONTRIBUTIONS
GS, LZ, AM, and SG designed research; GS, LZ, MM, WG, SB, AS, JG, AM, and SG performed research; GS, LZ, MM, WG, AT, SB, KB, AS, JG, AM, SG analyzed data; and GS, LZ, MM, AT, KB, AS, JG, AM, and SG wrote the manuscript.

COMPETING INTERESTS
The authors declare no competing interests.

ADDITIONAL INFORMATION
Supplementary information The online version contains supplementary material available at https://doi.org/10.1038/s43705-023-00314-9.

Correspondence and requests for materials should be addressed to Scott Gifford.

Reprints and permission information is available at http://www.nature.com/reprints

Publisher's note Springer Nature remains neutral with regard to jurisdictional claims in published maps and institutional affiliations.